J|A|C|S COMMUNICATIONS

Published on Web 07/13/2010

# Temperature-Responsive Nanospheres with Bicontinuous Internal Structures from a Semicrystalline Amphiphilic Block Copolymer

Beulah E. McKenzie,[†] Fabio Nudelman,[‡] Paul H. H. Bomans,[‡] Simon J. Holder,*[,†] and Nico A. J. M. Sommerdijk*[,‡]

*Functional Materials Group, School of Physical Sciences, University of Kent, Canterbury, Kent CT2 7NH, U.K., and Laboratory of Materials and Interface Chemistry and Soft Matter Cryo-TEM Research Unit, Eindhoven University of Technology, P.O. Box 513, 5600 MB Eindhoven, The Netherlands*

Received March 17, 2010; E-mail: S.J.Holder@kent.ac.uk; N.Sommerdijk@tue.nl

***Abstract:*** Internally structured self-assembled nanospheres, cubosomes, are formed from a semicrystalline block copolymer, poly(ethylene oxide)-*block*-poly(octadecyl methacrylate) ($PEO_{39}$-*b*-$PODMA_{17}$), in aqueous dispersion. The PODMA block provides them with a temperature-responsive structure and morphology. Using cryo-electron tomography, we show that at room temperature these internally bicontinuous aggregates undergo an unprecedented order−disorder transition of the microphase-separated domains that is accompanied by a change in the overall aggregate morphology. This allows switching between spheres with ordered bicontinuous internal structures at temperatures below the transition temperature and more planar oblate spheroids with a disordered microphase-separated state above the transition temperature. The bicontinuous structures offer a number of possibilities for application as templates, e.g., for biomimetic mineralization or polymerization. Furthermore, the unique nature of the thermal transition observed for this system offers up considerable possibilities for their application as temperature-controlled release vessels.

Amphiphilic AB and ABA block copolymers have been demonstrated to form a variety of self-assembled aggregate structures in dilute solutions where the solvent preferentially solvates one of the blocks.[1] The most common structures formed by these amphiphilic macromolecules are spherical micelles, cylindrical micelles, and vesicles (polymersomes), with the type of aggregate depending principally upon the relative volumes of the different blocks.[1] Over the past decade, more complex aggregate structures have been observed and targeted for construction. The majority of these aggregates (such as disk-like and toroidal micelles) may be grouped under the description of complex micelles and can be achieved both through manipulating block copolymer structures and through physical means.[2] Multicompartment micelles are typically the result of ABC block copolymers, of which one of the blocks is solvophilic and the remaining two are solvophobic but do not mix.[3] Hence, microphase-separated micellar cores result.

We recently reported the experimental observation of complex micelles with bicontinuous hydrophilic/hydrophobic internal structures from amphiphilic norbornene-based double-comb diblock copolymers, with a peptide and an oligo(ethylene oxide) side chain.[4] Block copolymer nanoparticles with similar bicontinuous phase separation have also been observed by Wooley et al.[5] and before that were predicted by Fraaije and Sevink.[6] In the present paper we demonstrate the formation of similar complex micelles, with hydrophobic bicontinuous internal morphologies from an amphiphilic semicrystalline AB(C) comb-like block copolymer. Using cryo-electron tomography, we show that at room temperature these internally structured nanoparticles undergo an unprecedented order−disorder transition involving the reorganization of the microphase-separated domains that is accompanied by a change in the overall aggregate morphology.

***Scheme 1.*** Chemical Structure (Top) and 3D Represenatation (Bottom) of $PEO_{39}$-*b*-$PODMA_{17}$

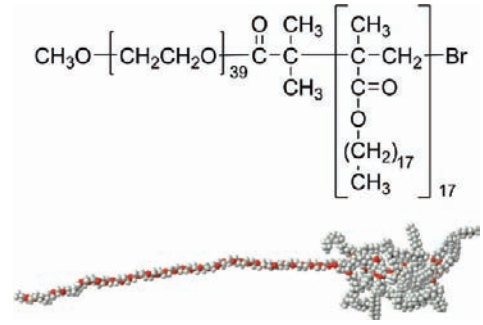


A new AB(C) amphiphilic block copolymer, poly(ethylene oxide)-*block*-poly(octadecyl methacrylate) ($PEO_{39}$-*b*-$PODMA_{17}$, $M_n$ = 7680, $M_w/M_n$ = 1.11, wt $\%_{PEO}$ = 25) was synthesized by the atom-transfer radical polymerization (ATRP) of ODMA from a PEO macroinitiator (Scheme 1 and Supporting Information (SI)). Differential scanning calorimetry (DSC) studies showed two melting transitions for the bulk material, the first at 24.2 °C (PODMA) and the second at 31.3 °C (PEO) (SI). Aggregate dispersions of this copolymer were formed by slow addition of 6 mL of water to 4 mL THF solutions at 35 °C and subsequent dialysis against water at 35 °C over 24 h to give 1 and 5 wt % aggregate dispersions in 10 mL of water (SI).[7] The initial solutions went from transparent to white translucent during water addition, indicating preliminary aggregation of the copolymer during this process; the solutions became opaque white during subsequent dialysis. Negative staining transmission electron microscopy (TEM) demonstrated that, at room temperature, spherical aggregates were present with diameters of 200 ± 100 nm for the 1 wt % and 450 ± 150 nm for the 5 wt % solutions (SI). Dynamic light scattering (DLS) studies of the solutions at 35 °C gave number-average diameters of 343 nm (dispersity = 0.366) for the 5 wt % and 276 nm (dispersity = 0.310) for the 1 wt % solutions. DSC analysis of the 5 wt % solution revealed an endothermic thermal transition with a $T_{trans}$ = 21.8 °C on heating and a $T_{trans}$ = 7.8 °C on cooling (peak maxima, Figure 1a,b). These transitions are tentatively assigned to the melting and crystallization of portions of the octadecyl chains in the aggregates.[8]

[†] University of Kent.
[‡] Eindhoven University of Technology.

 **10.1021/ja102040u** 

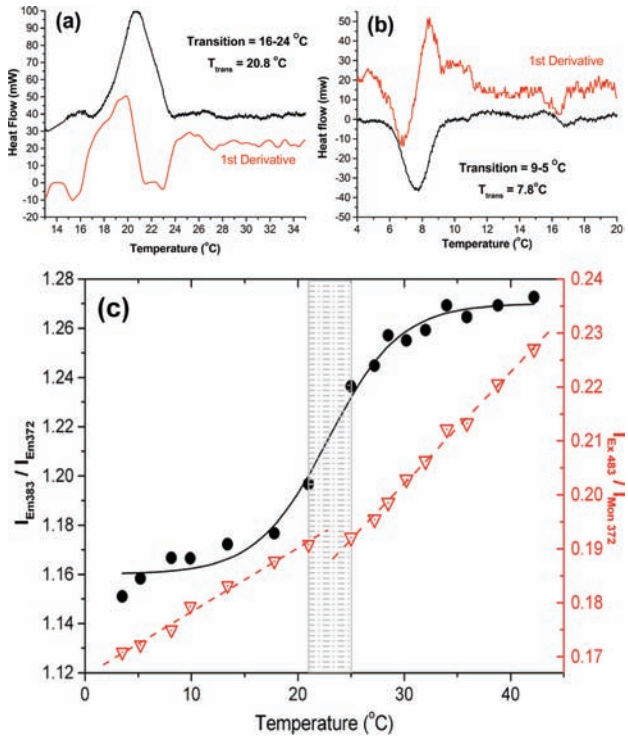


***Figure 1.*** DSC traces of 5 wt % solution of PEO−PODMA aggregates during a 10 K $min^{-1}$ (a) heating run and (b) cooling run. (c) Variation with temperature of ratios of the III:I ($I_{Em383}/I_{Em372}$) bands and the $I_{exc}$:$I_{mon}$ ($I_{Ex483}/I_{Mon372}$) bands for pyrene encapsulated in 1 wt % aggregate solutions.

The structure and thermal behavior of these aggregates were further investigated with cryoTEM and cryo-electron tomography (cryoET − 3D cryoTEM). The 2D cryoTEM projection images of the 5 wt % solution vitrified at 4 °C showed numerous round aggregates that possessed an ordered internal microphase-separated structure (Figure 2a, and SI Figures S10a and S11). Samples vitrified at the transition point (22 °C) showed spherical aggregates with a variety of internal structures with lower apparent order compared to the those present at 4 °C (SI Figures S10b and S12). Also the projection images recorded at 45 °C showed round objects; however, these showed poor contrast with the surrounding vitrified ice matrix, and an ordered internal structure could no longer be observed (Figure 2e, and SI Figures S10c and S13). CryoET was performed by recording tilt series of 85−95 cryoTEM images of the vitrified samples between −70° and +70° with increments of 2° at low angles and 1° at high angles and subsequently reconstructing the investigated volume using a simultaneous iterative reconstruction technique (SIRT) algorithm (Figure 2b). The 3D visualization of the reconstructed volumes revealed that below $T_{trans}$ the aggregates were spherical and predominantly possessed a sponge-like structure, consisting of an ordered bicontinuous network of intertwined water-filled and carbon-rich channels (both ∼13 nm in thickness/diameter), in which the aqueous channels were in contact with the surrounding medium (Figure 2c,d, and SI Figure S15). While the majority structural component of the aggregates at 4 °C was observed to be bicontinuous, some internal lamellar organization was observed in places (Figure 2c). While the origin of the lamellar regions remains unknown, its coexistence with the bicontinuous morphology suggests that the aggregates' internal structure may lie at a hypothetical phase boundary between the two microphase-separated states.[9] The tilt series (Figure 2f, and SI Figure S14) and 3D reconstructions (Figure 2g) of the aggregates at 45 °C still showed some residual but highly disordered microphase-separated structure (again with ∼13 nm dimensions) in the interior of aggregates vitrified at temperatures above $T_{trans}$. These 3D images also revealed that the aggregates were not spherical but had a flattened, oblate spheroidal shape.

In line with DSC data obtained for solution and bulk samples of the block copolymer. we suggest that above $T_{trans}$ an order−disorder transition is taking place that accompanies the melting of the octadecyl chains. Furthermore, the tomograms showed that during the thermal transition the aggregates flatten to a more planar oblate spheroid morphology which, along with the now completely amorphous nature of the block copolymer, explains the reduced electron density observed in the 2D images. Unfortunately, the resolution and contrast of the reconstructions did not allow us to determine whether the observed residual compartments were interconnected throughout the interior of the aggregates, as was the case below $T_{trans}$. CryoTEM and cryoET of the 1 wt % solution above and below $T_{trans}$ gave results similar to those observed for the 5 wt % solution, although the degree of order at 4 °C and the microphase separation at 45 °C were less pronounced (SI Figures S8 and S9).

Variable-temperature fluorescence spectroscopy of a 1 wt % aggregate solution containing encapsulated pyrene (py) revealed marked changes in the intensities of both the py monomer signals ($I_{mon}$) and the excimer peak ($I_{exc}$) in the temperature range of 17−25 °C (Figure 1c, and SI Figure S18), indicating significant changes in the environment of the probe molecues.[10] The transition in this temperature range closely matches that observed by DSC for the 5 wt % solution. The midpoint of the $I_{III}/I_I$ sigmoidal plot is 22.9 °C, and the intersection of the slopes for the $I_{exc}/I_{mon}$ plot is 23.1 °C (Figure 1c). Both values are very close to the $T_{trans}$ of 21.8 °C, providing confirmation for a change in structure of the microphase-separated state deduced from the observed transition temperature recorded by DSC and images from TEM. The increase in the pyrene $I_{III}/I_I$ ratio from ∼1.16 to 1.26 indicates a decrease in the polarity (an increase in the hydrophobicity) of the environment of the probe.[11,12] The change in the slope of the $I_{exc}/I_{mon}$ vs $T$ plot at ∼22−25 °C (Figure 2c) is indicative of a decrease of the microviscosity in the py environment.[10,13] Since py is excluded from the crystalline portions of semicrystalline polymers, these observations support the postulate that, at $T_{trans}$ upon heating, the crystalline segments of the octadecyl chains melt, resulting in py dilution in the chains and reduced proximity to the polar C═O groups (Figure 3).[14] The resultant entirely amorphous PODMA phase will have an increased hydrophobicity, in agreement with the observed increase in $I_{III}/I_I$ ratio. This leads to a higher probe mobility, as associated with the semicrystalline-to-amorphous transition in the polymer and in line with the more rapid increase of the $I_{exc}/I_{mon}$ ratio observed in the temperature range of 22−25 °C. While the presence of crystalline regions is not needed for the formation of these large microphase-separated aggregates (given that they are formed at 35 °C), it would appear that a degree of crystallinity is necessary for the formation of the bicontinuous morphology.

These internally structured self-assembled nanospheres that were only recently observed for the first time can be considered the polymeric analogues of cubosomes, aggregates that exhibit interior bicontinuous liquid crystalline order. Typically cubosomes are formed from low-molecular-weight compounds that are often present as mixtures and often require stabilizers.[15] These polymer cubosomes are now formed from a semicrystalline block copolymer which provides them with temperature-responsive structure and morphology. This allows switching between spheres with ordered bicontinuous internal structures at temperatures below the transition

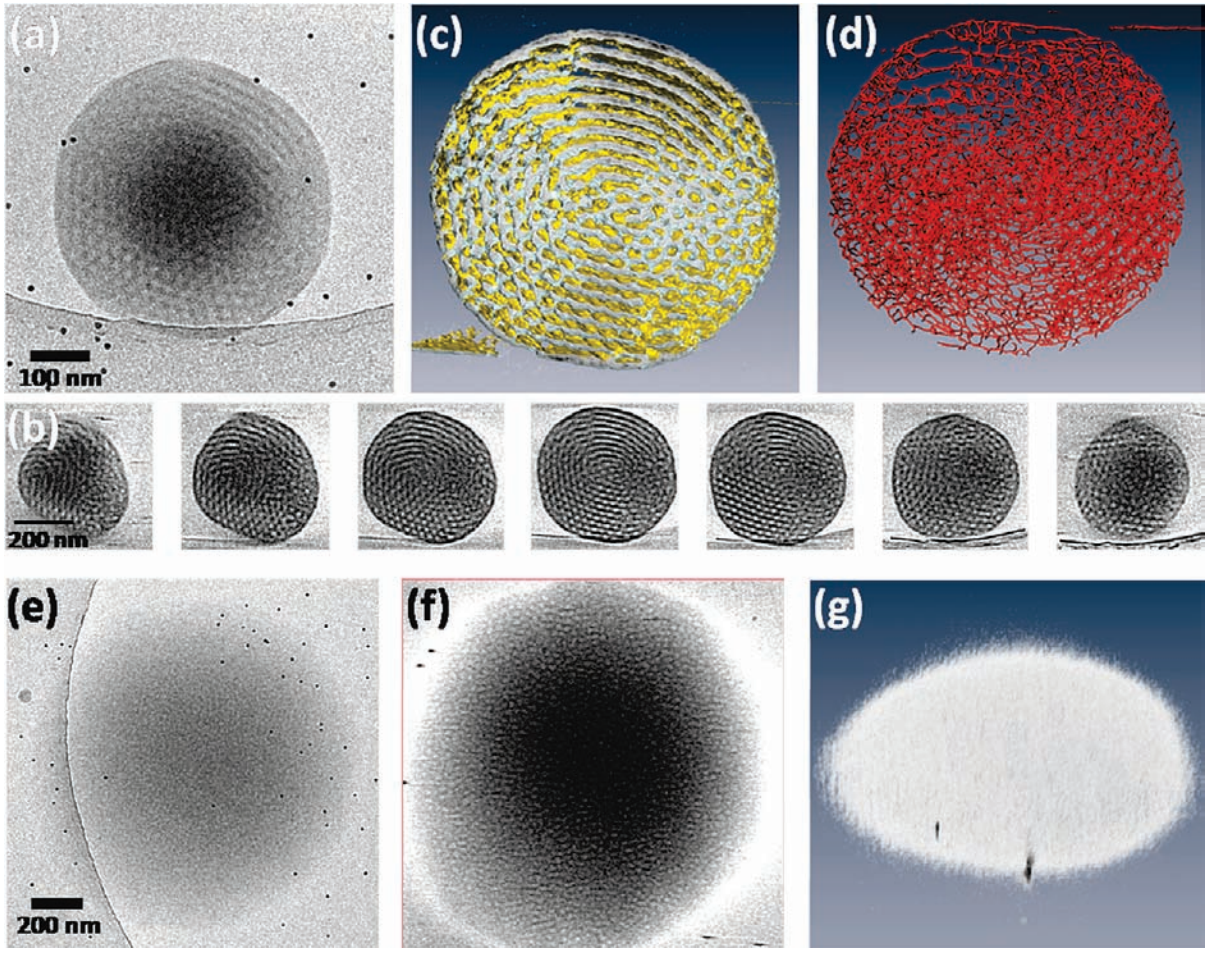


***Figure 2.*** TEM analysis of $PEO_{39}$-*b*-$PODMA_{17}$ aggregates: (a) cryoTEM image of a vitrified film at 4 °C; (b) gallery of *z* slices showing different cross sections of a 3D SIRT reconstruction of a tomographic series recorded from the vitrified film in (a); (c) computer-generated 3D visualization showing only an inner section of the whole structure, where all the channels and compartments are visible (the yellow surface is outside of the polymer, the surface in contact with the water); (d) skeletonization of (c), showing only a small section emphasizing that the structure is interconnected and therefore bicontinuous; (e) cryoTEM image of a vitrified film at 45 °C; (f) slice from a 3D SIRT reconstruction of a tomographic series recorded from the vitrified film in (e); and (g) volume rendering of the whole structure in (e), showing the overall morphology.

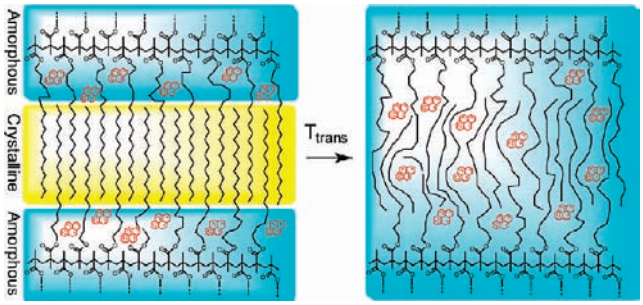


***Figure 3.*** Schematic representation of the melting of the crystalline portions of the octadecyl chains and the concomitant changes in the pyrene environment.

point and disk-like structures with a disordered microphase-separated internal composition above. The bicontinuous structures offer a number of possibilities for application as templates, e.g., for biomimetic mineralization or polymerization. Furthermore, the unique nature of the thermal transition observed for this system offers up considerable possibilities for their application as temperature-controlled release vessels.

**Supporting Information Available:** SI1, experimental details (Scheme S1, Figures S1−S5, and Table S1); SI2, DSC (Figure S6); SI3, DLS (Figure S7); SI4, cryoTEM (Figures S8−S15); and SI5, incorporation of pyrene (Figures S16−S18). This material is available free of charge via the Internet at http://pubs.acs.org.

## References

(1) (a) Tuzar, Z.; Kratochvil, P. In *Surface and Colloid Science*, Vol. 15; Matijevic, E., Ed.; Plenum Press: New York, 1993; p 1. (b) Discher, B. M.; Hammer, D. A.; Bates, F. S.; Discher, D. E. *Curr. Opin. Colloid Sci.* **2000**, *5*, 125–131. (c) Zhang, L.; Eisenberg, A. *Polym. Adv. Technol.* **1998**, *9*, 677–699. (d) Lutz, J. F. *Polym. Int.* **2006**, *55*, 979–993. (e) Gohy, J. F. *Adv. Polym. Sci.* **2005**, *190*, 65–136.

(2) (a) Chen, Z. Y.; Cui, H. G.; Hales, K.; Li, Z. B.; Qi, K.; Pochan, D. J.; Wooley, K. L. *J. Am. Chem. Soc.* **2005**, *127*, 8592–8593. (b) Pochan, D. J.; Chen, Z. Y.; Cui, H. G.; Hales, K.; Qi, K.; Wooley, K. L. *Science* **2004**, *306*, 94–97. (c) Yu, H. Z.; Jiang, W. *Macromolecules* **2009**, *42*, 3399–3404. (d) Li, Z. B.; Chen, Z. Y.; Cui, H. G.; Hales, K.; Qi, K.; Wooley, K. L.; Pochan, D. J. *Langmuir* **2005**, *21*, 7533–7539. (e) Gomez, E. D.; Rappl, T. J.; Agarwal, V.; Bose, A.; Schmutz, M.; Marques, C. M.; Balsara, N. P. *Macromolecules* **2005**, *38*, 3567–3570.

(3) (a) Li, Z. B.; Kesselman, E.; Talmon, Y.; Hillmyer, M. A.; Lodge, T. P. *Science* **2004**, *306*, 98–101. (b) Laschewsky, A. *Curr. Opin. Colloid Sci.* **2008**, *8*, 274–281. (c) Lutz, J.-F.; Laschewsky, A. *Macro. Chem. Phys.* **2005**, *206*, 813–817. (d) Weberskirch, R.; Preuschen, J.; Spiess, H. W.; Nuyken, O. *Macro. Chem. Phys.* **2000**, *201*, 995–1007. (e) Yabu, H.; Higuchi, T.; Shimomura, M. *Adv. Mater.* **2005**, *17*, 2062. (f) Okubo, M.; Takekoh, R.; Saito, N. *Colloid Polym. Sci.* **2004**, *282*, 1192. (g) Saito, N.; Takekoh, R.; Nakatsuru, R.; Okubo, M. *Langmuir* **2007**, *23*, 5978. (h) Cui, H.; Chen, Z.; Zhong, S.; Wooley, K. L.; Pochan, D. J. *Science* **2007**, *317*, 647.

(4) (a) Parry, A. L.; Bomans, P. H. H.; Holder, S. J.; Sommerdijk, N. A. J. M.; Biagini, S. C. G. *Angew. Chem., Int. Ed.* **2008**, *47*, 8859–8862.
(5) Hales, K.; Chen, Z.; Wooley, K. L.; Pochan, D. J. *Nano Lett.* **2008**, *8*, 2023.
(6) Fraaije, J. G. E. M.; Sevink, G. J. A. *Macromolecules* **2003**, *36*, 7891–7893.
(7) (a) Holder, S. J.; Durand, G. G.; Yeoh, C.-T.; Illi, E.; Hardy, N. J.; Richardson, T. H. *J. Polym. Sci. A: Polym. Chem.* **2008**, *46*, 7739–7756. (b) Holder, S. J.; Rossi, N. A. A.; Yeoh, C.-T.; Durand, G. G.; Boerakker, M. J.; Sommerdijk, N. A. J. M. *J. Mater. Chem.* **2003**, *13*, 2771–2778.
(8) Hempel, E.; Budde, H.; Horing, S.; Beiner, M. *J. Non-Cryst. Solids* **2006**, *352*, 5013–5020.
(9) Meuler, A. J.; Hillmyer, M. A.; Bates, F. S. *Macromolecules* **2009**, *42*, 7221–7250.
(10) (a) Duportail, G.; Lianos, P. In *Vesicles*; Rosoff, Ed.; M. Dekker: New York, 1996; p 295−372. (b) Metso, A. J.; Jutila, A.; Mattila, J.-P.; Hlopainen, J. M.; Kinnunen, P. K. J. *J. Phys. Chem. B* **2003**, *107*, 1251–1257. (c) Jung, M.; Hubert, D. H. W.; van Veldhoven, E.; Frederik, P. M.; Blandamer, M. J.; Briggs, B.; Visser, A. J. W. G.; van Herk, A. M.; German, A. L. *Langmuir* **2000**, *16*, 968–979.
(11) Waris, R.; Acree, W. E., Jr.; Street, K. W. *Analyst* **1988**, *113*, 1465–1467.
(12) Kalyanasundaram, K.; Thomas, J. K. *J. Am. Chem. Soc.* **1977**, *99*, 2039–2044.
(13) Aoudia, M.; Rogers, M. A. J.; Wade, W. H. *J. Phys. Chem.* **1984**, *88*, 5008–5012.
(14) Vigil, M. R.; Bravo, J.; Atvars, T. D. Z.; Baselga, J. *Macromolecules* **1997**, *30*, 4871–4876.
(15) (a) Larsson, K. *J. Phys. Chem.* **1989**, *93*, 7304–7314. (b) Larsson, K. *Curr. Opin. Colloid Interface Sci.* **2000**, *5*, 64–69. (c) Bucheim, W.; Larsson, K. *J. Colloid Interface Sci.* **1987**, *117*, 582–583. (d) Larsson, K. *J. Phys. Chem.* **1989**, *93*, 7304–7314. (e) Landh, T. *J. Phys. Chem.* **1994**, *98*, 8453–8467. (f) Spicer, P. T. *Curr. Opin. Colloid Interface Sci.* **2005**, *10*, 274. Barauskas, J.; Johnsson, M.; Tiberg, F. *Nano Lett.* **2005**, *5*, 1615. (g) Barauskas, J.; Johnsson, M.; Joabsson, F.; Tiberg, F. *Langmuir* **2005**, *21*, 2569.

JA102040U